A Low Computational Burden Model Predictive Control for Dynamic Wireless Charging

Tianlu Ma, *Student Member*, *IEEE*, C. Q. Jiang, *Senior Member, IEEE*, Chen Chen, Yibo Wang, Jiayi Geng, and Chi K. Tse, *Fellow, IEEE*

***Abstract*—Dynamic wireless charging (DWC) technology can help alleviate the problem of short driving range for battery-powered vehicles. In this paper, a model predictive control (MPC) is applied to the buck converter on the secondary side of a DWC system to address fast output fluctuations. This approach features a fast dynamic response, and no communication link is required. To solve the key issue of MPC, which is the computational burden, a polynomial fitting method based on the parsing solution of the sampled-data model is proposed. The complex matrix exponential calculation is replaced by simple polynomial operations, and the optimal duty cycle can be calculated directly by solving a quadratic function. This significantly reduces the computational burden. A DWC experimental setup is constructed, and results show that the proposed MPC has a better dynamic performance compared to proportional-integral control. The adjustment time is only 140 μs (around seven switching cycles) when the reference voltage is stepping. Moreover, the computational burden for matrix calculation in two-step prediction can be reduced by 50.6% and 79.7% compared to the lookup table and Taylor series approximation, respectively. Meanwhile, MPC with current limitation is analyzed and demonstrates a neat spectrum, small ripple but large response time.**

***Index Terms*— DC-DC converters, dynamic wireless charging (DWC), model predictive control (MPC), sampled-data model, and wireless power transfer (WPT).**

I. INTRODUCTION

WIRELESS power transfer (WPT) systems have been applied to many appliances, such as smartphones [1], electric vehicles [2], and automatic guided vehicles [3]. They will continue to attract attention due to their safety, reliability, low maintenance cost, and convenience of use. In order to alleviate the problem of short driving range, wireless charging for devices such as warehouse robots is an effective solution that does not require the use of large batteries.

Dynamic wireless charging (DWC) technology can be classified into two types based on the type of magnetic coupler used on the primary side. The first type is the long track coupler [4], where the primary coil is much longer than the receiving coil, resulting in a lower coupling coefficient and transmission efficiency. Additionally, this type of DWC faces the challenge of electromagnetic interference (EMI). The second type is the segmented coupler [5], which features multiple transmitting coils on the primary side that are similar in size to the receiving coil. This type of DWC offers higher transmission efficiency compared to the long track coupler. However, using multiple transmitters can lead to increased costs and require complex control.

In order to compensate for the reactive power and improve transmission efficiency, compensation networks are always needed on both the primary and secondary sides [6]. There are four basic compensation networks, namely, series-series (SS) [7], [8], series-parallel (SP) [9], parallel-series (PS) [10], and parallel-parallel (PP) [11]. The selection of the appropriate compensation network depends on the specific system characteristics and the desired performance goals. High-order compensation networks are used widely because they have better performance in some areas. For example, inductor–capacitor–inductor (LCL) compensation network [12] and inductor–capacitor–capacitor (LCC) [13] compensation networks are applied more frequently in the DWC system because they can excite a constant current on the transmitting coil. This is particularly beneficial in DWC systems where the load and coupling conditions may vary. In addition, compared to the LCL compensation network, the LCC compensation network helps to reduce voltage stress on the components, which can enhance the overall reliability and lifespan of the system.

The critical feature of the DWC system is that the mutual inductance or coupling coefficient will vary when the receiver moves. The varying mutual inductance will cause a power fluctuation on the receiver, which is a key issue that needs to be addressed. The first solution is to optimize the couplers to excite uniform magnetic fields [14]-[18]. In a recent analysis of the coupling coefficient between adjacent coils with respect to transmitter space [14], the coupling coefficient has always been found to be negative for adjacent coils without overlap. When adjacent coils are close together, and the receiving coil is 1.25 times the length of the transmitting coil, the overall coupling coefficient has the minimum fluctuation. A grouped periodic series spiral coupler was proposed in [15]. Coil arrays were both adopted on the transmitter and receiver, and the switches

Manuscript received July 26, 2023; revised September 26, 2023; accepted December 6, 2023. This work was supported in part by the Science Technology and Innovation Committee of Shenzhen Municipality, China, under Grant SGDX20210823104003034, in part by the Natural Science Foundation of China, China, under Grant 52107011, in part by the Research Grants Council, Hong Kong SAR under ECS Grant 21200622, in part by the City University of Hong Kong under TDG 6000791. (*Corresponding author: C. Q. Jiang*)

Tianlu Ma, C. Q. Jiang, Chen Chen, Yibo Wang, and Jiayi Geng are with the Department of Electrical Engineering and the State Key Laboratory of Terahertz and Millimeter Waves, City University of Hong Kong, Hong Kong, China. Also, they are with City University of Hong Kong Shenzhen Research Institute, Shenzhen 518057, China. (e-mail: tianlu.ma@my.cityu.edu.hk; chjiang@cityu.edu.hk; chen.chen@my.cityu.edu.hk; yibo.wang@my.cityu.edu.hk; jiayi.geng3@unibo.it).

Chi K. Tse is with the Department of Electrical Engineering, City University of Hong Kong, Hong Kong, China. (e-mail: chitse@cityu.edu.hk).

increased with the number of coils, resulting in low robustness despite improved the ability of anti-positional offset. In addition, a new coil structure, DD coils and Q coil placed alternately, was presented in the DWC system [16]. The mutual inductance between adjacent transmitters could be neglected by using this structure. Therefore, the compensation network of each transmitter can be designed independently. A three-phase inverter was used to supply power for three adjacent transmitting coils in [17], and a 120-degree phase difference between adjacent coils could make the magnetic field variation smaller. Furthermore, a magnetic integrated method was applied for the magnetic coupler against power fluctuation [18]. A reverse coil was connected in series with the transmitting coil and was integrated with the transmitter, and its width was optimized to minimize the mutual inductance fluctuation.

To address mutual inductance fluctuation, another approach is to stabilize the output using a control method [19]-[21]. A current amplitude modulation method was proposed to optimize the transmitter current distribution through an n-spherical coordinate analogy [19]. The overall performance of the system was improved, and the negative effects of misalignment were also alleviated. Also, a primary-side-only control was presented to stabilize output power [20]. There is no dual-side wireless communication and hardware circuit on the secondary side, which can save space and improve the system's robustness. Moreover, the passivity-based proportional-integral (PI) control was proposed for the DWC system, and it was proved to have a better performance against mutual inductance variation than the conventional proportional-integral-derivative (PID) controller [21].

Model predictive control (MPC) is widely used in power electronics circuits due to its fast response and intuitive framework, which can be used to overcome the rapid fluctuations on the secondary side of DWC systems. An offset-free composite MPC strategy for the buck converter was proposed in [22]. A higher-order sliding mode observer was applied to evaluate the future tracking error to deal with the model uncertainties. However, its application was limited to constant power loads. MPC can also be applied to more complex converter circuits. In [23], MPC was used for the dual active bridge (DAB) with triple-phase shift, and two sampling periods were covered, considering the computational delay. Also, a lookup table method for MPC was proposed in [24] to save computing time. Meanwhile, huge memory consumption was required for highly accurate prediction. Moreover, two new MPC strategies, one-step and two-step prediction, were compared in [25] for grid-connected AC-DC converters with LCL filters. The two-step algorithm has a better performance than the one-step one, and a low total harmonic distortion was realized in both.

A primary-side MPC control strategy was used for the WPT system with a fast dynamic response in [26]. The system's mathematical model was established by fundamental harmonic approximation (FHA). However, the load needed to be estimated due to no communication link, and only phase-shift modulation was analyzed. An MPC control strategy was applied to the active rectifier of the WPT system [27], and FHA was employed to derive the dynamic model to estimate output voltage. However, the accuracy of FHA is low when there are high-frequency harmonics during system operation. A buck converter was added on the secondary side of a DWC system, and MPC was executed in the buck converter based on the state average model [28]. The sampling delay could be compensated if it equals integer multiples of the switching cycle. However, multi-step prediction and multi-cycle delay compensation mean that the computational burden also increases exponentially.

MPC has been proven to have a faster response than PID control [27], [28]. However, since MPC relies on a high-accuracy model, mitigation of the computational burden is a critical issue to address. In this paper, an MPC with a low computational burden is proposed and applied to the buck converter on the secondary side of DWC systems to realize the fast response and suppress power fluctuations. The computational burden for matrix calculation in two-step prediction can be reduced by 50.6% and 79.7% compared to the lookup table method [24] and Taylor series approximation. A DWC system of 2000 mm long and 400 mm wide with five transmitters and one receiver is built, and no communication is needed on the primary and secondary sides when using the proposed MPC. The contributions are listed as follows:

1) The parsing solution of the sampled-data model for the buck converter on the secondary side of the DWC system is derived through matrix exponential diagonalization.
2) A polynomial fitting with high accuracy is proposed and achieved based on the parsing solution of the mathematical model, and fitting results can be used to predict the system trajectory with a low computational burden.
3) The optimal duty cycle is obtained directly by solving a quadratic function instead of solving a cost function, which can reduce the computational complexity further.

In Section II, the DWC system and its equivalent circuit are described. In Section III, the sampled-data model of the buck converter is built, and the parsing solution is derived based on system parameters. The polynomial fitting is applied to the input matrix to reduce the calculation complexity. In Section IV, MPC with a one-step delay is illustrated, the optimal duty cycle is solved by the fitting function directly, and the current limitation is analyzed. In Section V, experiments are presented to verify the effectiveness of the proposed MPC. A conclusion is drawn in Section VI.

II. Dynamic Wireless Power Transfer Systems

A dc-dc converter is often added in the primary as well as the secondary sides of a stationary WPT system to realize the control targets. Similarly, for the DWC system, since the position between transmitters and receivers would change while the receivers move fast, the output will fluctuate rapidly at the same time. In this paper, a dc-dc converter is added between the rectifier and the load. Meanwhile, an MPC strategy is proposed and executed in a dc-dc converter on the secondary without any communication link.

An example of DWC for warehouse robots is shown in Fig. 1, and the robots can be charged when they are moving.

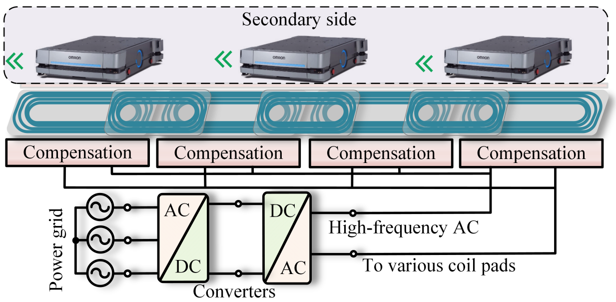

Fig. 1. The overall diagram of an example that dynamic wireless charging for warehouse robots.

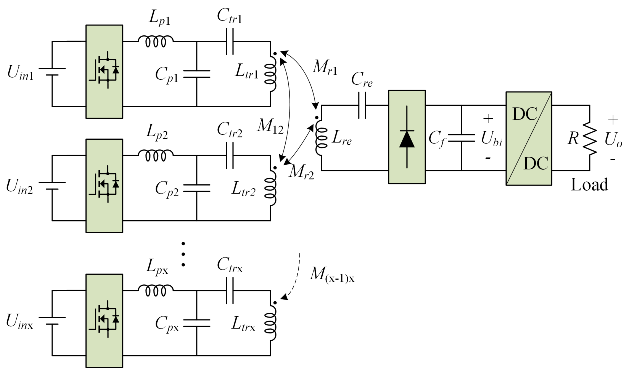

Fig. 2. Equivalent circuit of segmented DWC system with multiple independently controllable transmitters and one receiver.

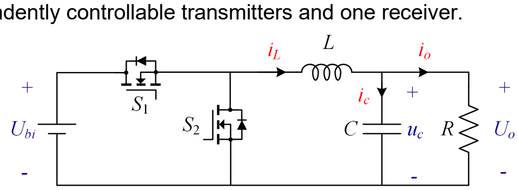

Fig. 3. Equivalent circuit of the synchronous buck converter.

Therefore, a high working efficiency can be realized. Also, DWC is suitable for other devices, like electric vehicles. The equivalent circuit of the segmented DWC system is shown in Fig. 2. The LCC compensation network is used on the primary sides, which can keep the transmitter current constant, and a simple series compensation network is used on the secondary side. L_{px}, C_{px}, and C_{trx} are composed of LCC-compensation networks, and L_{trx} is the self-inductance of the transmitting coil. L_{re} is the self-inductance of the receiving coil, C_{re} is the series compensation capacitor on the secondary side, C_f is the filter capacitor, U_{inx} is the input voltage, and R is the equivalent load resistance. In addition, M_{rx} is the mutual inductance between the receiver and the transmitter, and $M_{(x\text{-}1)x}$ is the mutual inductance between nearby transmitting coils.

The compensation networks on the primary and secondary sides follow as

$$\begin{cases} j\omega L_{px} = -\dfrac{1}{j\omega C_{px}} \\ j\omega L_{px} = \dfrac{1}{j\omega C_{trx}} + j\omega L_{trx} \\ j\omega L_{re} = -\dfrac{1}{j\omega C_{re}} \end{cases} \tag{1}$$

And the coupling coefficient between the x^{th} transmitter and receiver is expressed as

$$k_{rx} = M_{rx} \Big/ \sqrt{L_{trx} L_{re}} \tag{2}$$

The dc-dc converter can regulate the power flowing into the load by MPC with a fast response. The topology before the dc-dc converter is regarded as a black box, and the fluctuations and variations of the DWC system are bypassed. Therefore, no communication is needed for the control scheme proposed in this paper.

III. Polynomial Fitting for Sampled-data Model

A. Sampled-data Model of Buck Converters

The equivalent circuit of the buck converter is shown in Fig. 3. The switch S_1 will control the power flowing into the load. The sampled-data model will be established according to the switching state. Assume that the input and output voltage are constant in each switching period. When switch S_1 turns on, the circuit equations are derived based on the equivalent circuit, i.e.,

$$\begin{cases} U_{bi} = L\dfrac{di_L(t)}{dt} + U_o \\ i_c(t) = C\dfrac{du_c(t)}{dt} \\ i_L(t) = i_c(t) + i_o(t) \\ u_c(t) = U_o(t) = i_o(t)R \end{cases} \tag{3}$$

State equations for two switching states (S_1 on or off) are

$$\begin{cases} \dot{\boldsymbol{x}}(t) = \boldsymbol{A}_1\boldsymbol{x}(t) + \boldsymbol{B}_1 U_{bi}, & nT_s \le t < nT_s + dT_s \\ \dot{\boldsymbol{x}}(t) = \boldsymbol{A}_2\boldsymbol{x}(t) + \boldsymbol{B}_2 U_{bi}, & nT_s + dT_s \le t < (n+1)T_s \end{cases} \tag{4}$$

where the state vector $\boldsymbol{x}(t) = [i_L(t), u_c(t)]^T$, T_s is the switching period, d is the duty cycle of the driving signal of switch S_1, and the matrices are

$$\boldsymbol{A}_1 = \boldsymbol{A}_2 = \begin{bmatrix} 0 & -1/L \\ 1/C & -1/(RC) \end{bmatrix}, \boldsymbol{B}_1 = \begin{bmatrix} 1/L \\ 0 \end{bmatrix}, \boldsymbol{B}_2 = \begin{bmatrix} 0 \\ 0 \end{bmatrix}$$

The circuit connections are the same for these two states. Therefore, the system matrices are the same, namely, $\boldsymbol{A}_1 = \boldsymbol{A}_2$. And the input matrix $\boldsymbol{B}_2$ will be zero because switch S_2 bypasses the power supply. The solution of these two state equations are

$$\begin{cases} \boldsymbol{x}(t) = e^{\boldsymbol{A}_i t} x(0) + \boldsymbol{\psi}_i U_{bi} \\ \boldsymbol{\psi}_i = \int_0^{t_{ni}} e^{\boldsymbol{A}_i (t_{ni} - \tau)} \boldsymbol{B}_i d\tau = \boldsymbol{A}_i^{-1}\left(e^{\boldsymbol{A}_i t_{ni}} - \boldsymbol{I}\right)\boldsymbol{B}_i \end{cases} \tag{5}$$

where $i = 1,2$, $t_{n1} = dT_s$, $t_{n2} = (1\text{-}d)T_s$, $\boldsymbol{I}$ is the identity matrix of order 2, and $\boldsymbol{x}(0)$ is the initial state variables. There are two state intervals in each switching period, and the sampled-data model for each switching period can be obtained by iteration.

$$\boldsymbol{x}_{n+1} = \boldsymbol{F}(d)x_n + \boldsymbol{G}(d)U_{bi} \tag{6}$$

where the matrices are

$$\begin{cases} \boldsymbol{F}(d) = e^{\boldsymbol{A}_2 t_{n2}} e^{\boldsymbol{A}_1 t_{n1}} = e^{\boldsymbol{A}_1 T_s} = e^{\boldsymbol{A}_2 T_s} \\ \boldsymbol{G}(d) = e^{\boldsymbol{A}_2 t_{n2}} \boldsymbol{\psi}_1 + \boldsymbol{\psi}_2 = e^{\boldsymbol{A}_2 t_{n2}} \boldsymbol{A}_1^{-1}\left(e^{\boldsymbol{A}_1 t_{n1}} - \boldsymbol{I}\right)\boldsymbol{B}_1 \end{cases} \tag{7}$$

Since the output voltage equals the capacitor voltage, the output equation can be expressed as

$$U_{on} = \boldsymbol{T}\boldsymbol{x}_n \tag{8}$$

where $\boldsymbol{T} = [0, 1]$. It is difficult to calculate matrix exponential reliably and accurately, which is still a topic of considerable research in mathematics. Parsing solution for the sampled-data model in (6) is desired for MPC in the next section. In addition, if a matrix is diagonal, its exponential can be solved by

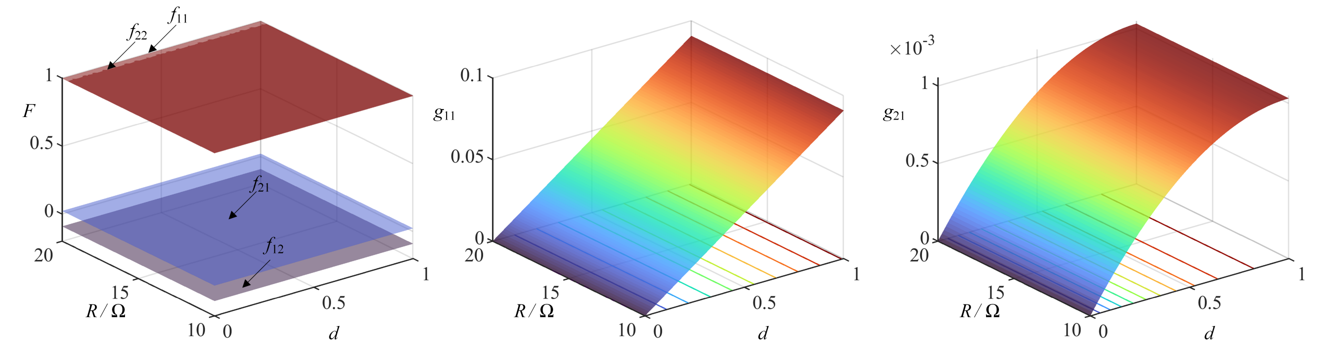

(a) (b) (c)

Fig. 4. Elements of the system matrix and input matrix versus load resistor and duty cycle. (a) Four elements of the system matrix. (b) The first element of the input matrix. (c) The second element of the input matrix.

TABLE I. SENSITIVITY OF EACH ELEMENT OF MATRIX ***F*** AND ***G*** TO SYSTEM PARAMETERS

Parameter X	$S_X^{f_{11}}$	$S_X^{f_{12}}$	$S_X^{f_{21}}$	$S_X^{f_{22}}$	$S_X^{g_{11}(d)}$	$S_X^{g_{21}(d)}$
L	1.03×10^{-3}	0.9997	3.45×10^{-4}	1.03×10^{-3}	0.9990 - 0.9997	0.9997 - 0.9998
C	1.03×10^{-3}	1.48×10^{-3}	0.9986	3.31×10^{-3}	3.44×10^{-4} - 1.02×10^{-3}	0.9985 - 0.9991
R	7.82×10^{-7}	1.14×10^{-3}	1.14×10^{-3}	2.27×10^{-3}	1.96×10^{-7} - 7.71×10^{-7}	7.57×10^{-4} - 1.13×10^{-3}

Note: The sensitivity is based on system parameters of L = 220 μH, C = 880 μF, and R = 10 Ω.

exponentiating each entry on the main diagonal. As a result, the matrix exponential can be calculated by

$$e^{\boldsymbol{A}} = \boldsymbol{U}e^{\boldsymbol{D}}\boldsymbol{U}^{-1} \tag{9}$$

if $\boldsymbol{A} = \boldsymbol{UDU}^{-1}$ and $\boldsymbol{D}$ is diagonal. Matrix $\boldsymbol{D}$ is composed of characteristic roots, and matrix $\boldsymbol{U}$ consists of characteristic vectors. Therefore, the system matrix $\boldsymbol{A}_i$ will be diagonalized first to calculate the matrix exponential in the sampled-data model. The characteristic roots of matrix $\boldsymbol{A}_1$ and $\boldsymbol{A}_2$ can be derived as

$$\lambda_1 = \frac{-1+\sqrt{\left(L-4R^2C\right)/L}}{2RC}, \lambda_2 = \frac{-1-\sqrt{\left(L-4R^2C\right)/L}}{2RC} \tag{10}$$

And the matrix $\boldsymbol{U}$ and $\boldsymbol{D}$ can also be derived as

$$\boldsymbol{D} = \begin{bmatrix} \lambda_1 & 0 \\ 0 & \lambda_2 \end{bmatrix}, \boldsymbol{U} = \begin{bmatrix} 1 & 1 \\ -L\lambda_1 & -L\lambda_2 \end{bmatrix} \tag{11}$$

As a result, the constant matrix $\boldsymbol{F}$ can be calculated by

$$\boldsymbol{F} = e^{\boldsymbol{A}_1 T_s} = \boldsymbol{U}e^{\boldsymbol{D}T_s}\boldsymbol{U}^{-1} = \begin{pmatrix} \dfrac{\lambda_1 e^{T_s\lambda_2} - \lambda_2 e^{T_s\lambda_1}}{\lambda_1 - \lambda_2} & -\dfrac{e^{T_s\lambda_1} - e^{T_s\lambda_2}}{L\left(\lambda_1 - \lambda_2\right)} \\ \dfrac{L\lambda_1\lambda_2\left(e^{T_s\lambda_1} - e^{T_s\lambda_2}\right)}{\lambda_1 - \lambda_2} & \dfrac{\lambda_1 e^{T_s\lambda_1} - \lambda_2 e^{T_s\lambda_2}}{\lambda_1 - \lambda_2} \end{pmatrix} \tag{12}$$

and matrix $\boldsymbol{G}(d)$ can also be derived by

$$\begin{aligned} \boldsymbol{G}(d) &= e^{\boldsymbol{A}_2 t_{n2}}\boldsymbol{A}_1^{-1}\left(e^{\boldsymbol{A}_1 t_{n1}} - \boldsymbol{I}\right)\boldsymbol{B}_1 \\ &= \boldsymbol{U}e^{\boldsymbol{D}t_{n2}}\boldsymbol{U}^{-1}\boldsymbol{A}_1^{-1}\left(\boldsymbol{U}e^{\boldsymbol{D}t_{n1}}\boldsymbol{U}^{-1} - \boldsymbol{I}\right)\boldsymbol{B}_1 \\ &= \begin{bmatrix} \left(\dfrac{\sigma_6 - \sigma_7}{\sigma_3} + \dfrac{\sigma_5}{R}\right)\sigma_2 + \dfrac{C}{L}\sigma_5\sigma_1 \\ \left(\dfrac{L\left(\lambda_1\sigma_7 - \lambda_2\sigma_6\right)}{\sigma_3} + \dfrac{\sigma_4}{R}\right)\sigma_2 + \dfrac{C}{L}\sigma_4\sigma_1 \end{bmatrix} \end{aligned} \tag{13}$$

where

$$\sigma_1 = \frac{L\lambda_1\lambda_2\left(e^{T_s\lambda_1 d} - e^{T_s\lambda_2 d}\right)}{\lambda_1 - \lambda_2}, \sigma_2 = \frac{\lambda_2 e^{T_s\lambda_1 d} - \lambda_1 e^{T_s\lambda_2 d}}{\lambda_1 - \lambda_2} + 1, \sigma_3 = L\left(\lambda_1 - \lambda_2\right)$$

$$\sigma_4 = \frac{L\lambda_1\lambda_2\left(\sigma_7 - \sigma_6\right)}{\lambda_1 - \lambda_2}, \sigma_5 = \frac{\lambda_1\sigma_6 - \lambda_2\sigma_7}{\lambda_1 - \lambda_2}, \sigma_6 = e^{T_s\lambda_2(1-d)}, \sigma_7 = e^{T_s\lambda_1(1-d)}$$

Here, the sampled-data model has been expressed with the system parameters. Consequently, it can be calculated by (6), (12), and (13). Matrix $\boldsymbol{F}$ consists of constants, and matrix $\boldsymbol{G}(d)$ is related to the duty cycle. Also, they can be extended by

$$\boldsymbol{F} = \begin{bmatrix} f_{11} & f_{12} \\ f_{21} & f_{22} \end{bmatrix}, \boldsymbol{G}(d) = \begin{bmatrix} g_{11}(d) \\ g_{21}(d) \end{bmatrix} \tag{14}$$

The elements of the system matrix and input matrix with respect to the load resistor and the duty cycle are shown in Fig. 4, and the parameters of the buck converter used are shown in TABLE II. It should be noted that f_{11} and f_{22} are similar and close to 1, g_{11} is linear with the duty cycle, and g_{21} is a quadratic function of the duty cycle. System parameters, inductor L, capacitor C, and load resistor R, have completely different effects on matrix $\boldsymbol{F}$ and $\boldsymbol{G}$, which can be reflected by sensitivity analysis. The sensitivity of y to x is defined as

$$S_x^y = \left|\frac{\partial y/y}{\partial x/x}\right| = \left|\frac{x}{y}\frac{\partial y}{\partial x}\right| \tag{15}$$

Since matrix $\boldsymbol{F}$ is constant, the sensitivity of $\boldsymbol{F}$ to system parameters should also be constant. Whereas the sensitivity of $\boldsymbol{G}$ to system parameters is related to the duty cycle. The parameter sensitivities are summarized in TABLE I. It can be found that elements of matrix $\boldsymbol{F}$ and $\boldsymbol{G}$ all have small sensitivity to the load resistor.

B. Polynomial Fitting Based on Parsing Solution

The parsing solutions of the system matrix and input matrix in Part A require complex matrix exponential calculation, which increases the computational burden of the mathematical model. Therefore, a polynomial fitting method is applied to simplify the model calculation based on the parsing solution. The matrix $\boldsymbol{F}$ is a constant matrix, and its elements can be stored in the register of digital controllers and just read when used. The two elements of input matrix $\boldsymbol{G}$ depend on the duty cycle, and they can be fitted by a linear and quadratic function, i.e.,

$$\boldsymbol{G}(d) = \begin{bmatrix} g_{11}(d) \\ g_{21}(d) \end{bmatrix} \xrightarrow{\text{fitting}} \begin{cases} \hat{g}_{11}(d) = q_1 d + q_2 \\ \hat{g}_{21}(d) = p_1 d^2 + p_2 d + p_3 \end{cases} \tag{16}$$

where g_{11} and g_{21} are the first and second elements of input matrix $\boldsymbol{G}$, $\hat{g}_{11}$ and $\hat{g}_{21}$ are corresponding polynomial fitting

TABLE II. PARAMETERS OF THE BUCK CONVERTER

Symbol	Quantity	Value
L	Inductor	220 μH
C	Output filter capacitor	880 μF
R	Load resistance	10-20 Ω
f_s	Switching frequency	50 kHz

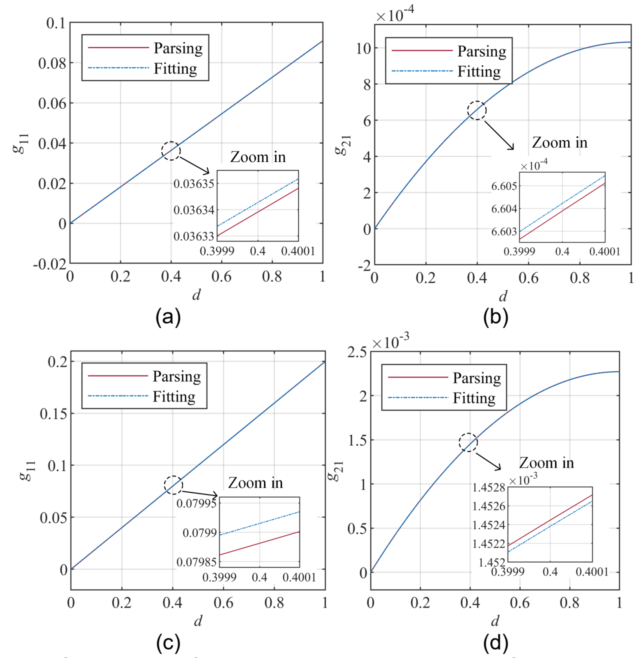

Fig. 5. Comparison of parsing solution and polynomial fitting when R = 10 Ω. (a) g_{11}, L = 220 μH.(b) g_{21}, L = 220 μH. (c) g_{11}, L = 100 μH.(d) g_{21}, L = 100 μH.

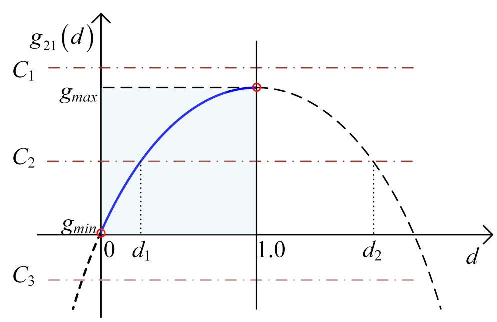

Fig. 6. Illustration of the optimal solution of duty cycle. (Note: $g_{21}(d)$ reaches maximum value at d = 1.)

results, and d is the duty cycle. The polynomial fitting can utilize the parsing solution in (13), and two key points, that the duty cycle is 0 and 1, are easily obtained, i.e.,

$$\boldsymbol{G}(0)=\begin{bmatrix} g_{11}(0) \\ g_{21}(0) \end{bmatrix}=\begin{bmatrix} 0 \\ 0 \end{bmatrix}, \boldsymbol{G}(1)=\begin{bmatrix} g_{11}(1) \\ g_{21}(1) \end{bmatrix}=\begin{bmatrix} \chi_1 \\ \chi_2 \end{bmatrix} \tag{17}$$

where

$$\begin{cases} \chi_1=\dfrac{C\lambda_1\lambda_2\left(e^{T_s\lambda_1}-e^{T_s\lambda_2}\right)}{\lambda_1-\lambda_2}+\dfrac{\lambda_2 e^{T_s\lambda_1}-\lambda_1 e^{T_s\lambda_2}}{R(\lambda_1-\lambda_2)}+\dfrac{1}{R} \\ \chi_2=\dfrac{\lambda_2 e^{T_s\lambda_1}-\lambda_1 e^{T_s\lambda_2}}{\lambda_1-\lambda_2}+1 \end{cases}$$

Two points are enough for the linear fitting function of $\hat{g}_{11}$, and another condition for the quadratic fitting function of $\hat{g}_{21}$ is that d = 1 is the symmetry axis of the quadratic fit function where g_{21} reaches its maximum value, i.e.,

$$d=1=-p_2/2p_1 \tag{18}$$

Plug (17) and (18) into (16), the polynomial fitting results can be derived as

$$\begin{cases} \hat{g}_{11}(d)=\chi_1 d \\ \hat{g}_{21}(d)=-\chi_2 d^2+2\chi_2 d \end{cases} \tag{19}$$

As a result, the elements of the input matrix are fitted by linear and quadratic functions. The coefficients of the fitting function are only related to the system parameters, which can be calculated and stored in the register of controllers before the system operation. Following the parameters in TABLE II, the fitting curves are compared with the parsing solution, as shown in Fig. 5. The goodness of fitting results can be evaluated by the sum of squared error (SSE); SSE is defined as

$$SSE=\sum_{i=0}^{n} w_i\left(y_i-f_i\right)^2 \tag{20}$$

where y_i is the observed data value, f_i is the value from fit, and w_i is the weighting that equals 1 in our work. SSE of g_{11} and g_{21} are equal to 7.45×10^{-9} and 1.09×10^{-12} for L = 220 μH, respectively, which validate high-accuracy fitting results.

To sum up, the system trajectory can be solved by simple polynomials instead of the complex matrix exponential. And the computational burden will be reduced dramatically for MPC in the next section. The fitting method to save computing time is also applicable to other isolated or non-isolated converters, although the input matrix and system need both fitting.

IV. MPC BASED ON POLYNOMIAL FITTING

A. MPC with One-step Delay

The state variables and output voltage at $(n+1)T_s$ can be predicted and calculated based on the state variables and duty cycle at nT_s, i.e.,

$$\begin{cases} \boldsymbol{x}_{n+1}^{pre}=\boldsymbol{F}x_n+\boldsymbol{G}(d_n)U_{bi} \\ U_{o(n+1)}^{pre}=\boldsymbol{T}\boldsymbol{x}_{n+1}^{pre} \end{cases} \tag{21}$$

As for the digital control circuit, it will take some time to sample and convert voltage and current by analog-to-digital converters (ADCs) in the digital controller. As a result, the duty cycle will be loaded into the register in the next switching period rather than be updated immediately. Therefore, a one-step delay should be considered for accurate and fast control, especially for high-frequency operations. The state variables and output voltage at $(n+2)$ T_s can be estimated by

$$\begin{cases} \boldsymbol{x}_{n+2}^{pre}=\boldsymbol{F}\boldsymbol{x}_{n+1}+\boldsymbol{G}(d_{n+1})U_{bi} \\ U_{o(n+2)}^{pre}=\boldsymbol{T}\boldsymbol{x}_{n+2}^{pre} \end{cases} \tag{22}$$

The duty cycle will be updated at the beginning of each switching period. However, the duty cycle should be loaded to the register before it is executed due to one step delay. Specifically, the duty cycle d_n will take effect at $t = nT_s$ and be executed during $nT_s \leqslant t < (n+1)T_s$, but it should be loaded to the register before $t = nT_s$. There are two assignments in the n^{th} switching period.

(a) The inductor current and capacitor voltage will be sampled at $t = nT_s$, and the state variable at $t = (n+1)T_s$ can be calculated by (21) based on the duty cycle d_n, which has been loaded into the register before $t = nT_s$.

(b) The optimal duty cycle $d_{opt(n+1)}$ during the next switching period, $(n+1)T_s \leqslant t < (n+2)T_s$, will be found

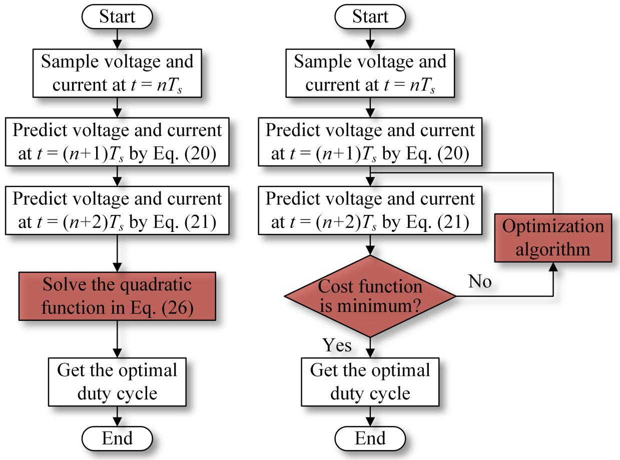

(a) (b)

Fig. 7. Flow charts of two kinds of MPC. (a) The proposed MPC with low computational burden. (b) Traditional MPC.

based on MPC, and then d_{opt} will be loaded into the register, which will be used in the next switching period.

B. Optimal Duty Cycle

Matrix $\boldsymbol{F}$ is a constant matrix, and four elements of matrix $\boldsymbol{F}$ can be stored in registers and just read them if needed. Also, matrix $\boldsymbol{G}(d)$ is fitted by a polynomial, and the values of its elements can be obtained quickly by (19). Therefore, the state variables at $(n+1)T_s$ can be estimated and calculated by (21) and it can be expanded by

$$\begin{bmatrix} i_{L(n+1)}^{pre} \\ u_{c(n+1)}^{pre} \end{bmatrix} = \begin{bmatrix} f_{11} & f_{12} \\ f_{21} & f_{22} \end{bmatrix} \begin{bmatrix} i_{Ln} \\ u_{cn} \end{bmatrix} + \begin{bmatrix} g_{11}(d_n) \\ g_{21}(d_n) \end{bmatrix} U_{bi} \tag{23}$$

Furthermore, the optimal duty cycle should be found quickly by quadratic function fitting in (19) to track the reference output voltage U_{ref}. The state variables at $(n+2)T_s$ can be predicted by

$$\begin{bmatrix} i_{L(n+2)}^{pre} \\ u_{c(n+2)}^{pre} \end{bmatrix} = \begin{bmatrix} f_{11} & f_{12} \\ f_{21} & f_{22} \end{bmatrix} \begin{bmatrix} i_{L(n+1)}^{pre} \\ u_{c(n+1)}^{pre} \end{bmatrix} + \begin{bmatrix} g_{11}(d_{n+1}) \\ g_{21}(d_{n+1}) \end{bmatrix} U_{bi} \tag{24}$$

Also, the output voltage at $(n+2)T_s$ can be expanded as

$$U_{o(n+2)}^{pre} = u_{c(n+2)}^{pre} = f_{21} i_{L(n+1)}^{pre} + f_{22} u_{c(n+1)}^{pre} + g_{21}(d_{n+1}) U_{bi} \tag{25}$$

Let the predicted output voltage equal to U_{ref}, and the optimal duty cycle can be solved by

$$g_{21}\left(d_{opt(n+1)}\right) = C = \frac{U_{ref} - f_{21} i_{L(n+1)}^{pre} - f_{22} u_{c(n+1)}^{pre}}{U_{bi}} \tag{26}$$

where C is a constant, and its value is determined by the system parameters and state variables at $(n+1)T_s$.

There are three cases for the solution of $d_{opt(n+1)}$ in (26), as shown in Fig. 6. The solution depends on the intersection of g_{21} and C. The effective zone of the duty cycle is from 0 to 1.0, and the maximum and minimum value of g_{21} in this range is g_{max} and g_{min}. The three cases are analyzed as follows.

(a) $C > g_{max}$. The optimal duty cycle will be 1.0, which supplies maximum power for the load.

(b) $g_{min} \leqslant C \leqslant g_{max}$. There will be two solutions, d_1 and d_2; the smaller d is the effective solution, i.e.,

$$d_1 = \left(p_2 - \sqrt{p_2^2 - 4p_1(p_3 - C)}\right) \Big/ (-2p_1) \tag{27}$$

(c) $C < g_{min}$. The optimal duty cycle will be 0, which supplies minimum power for the load.

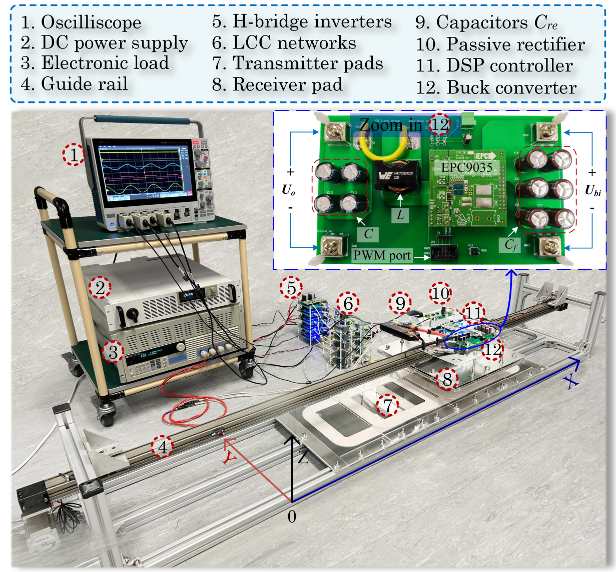

Fig. 8. Experimental setup of the dynamic system with five transmitters and one receiver.

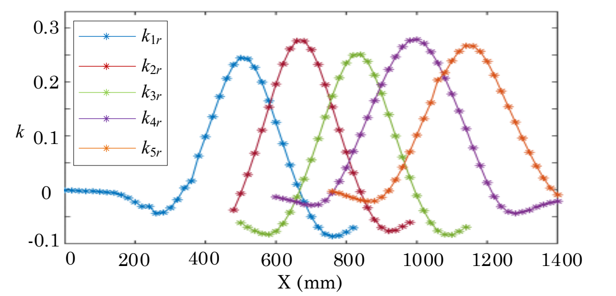

Fig. 9. Coupling coefficients between transmitters and receiver versus the position.

TABLE III. PARAMETERS OF THE DWC SYSTEM

Symbol	Quantity	Value
L_{tr1}-L_{tr5}	Transmitters self-inductance	223.80, 227.97, 230.34, 228.98, 223.16 μH
L_{p1}-L_{p5}	Primary compensated inductor	19.65, 19.57, 19.82, 19.57, 19.87 μH
C_{p1}-C_{p5}	Primary compensated capacitor 1	178.15,179.08, 176.72, 178.96, 176.45 nF
C_{tr1}-C_{tr5}	Primary compensated capacitor 2	17.59, 16.95, 17.55, 16.55, 17.65 nF
L_{re}	Receiver self-inductance	182.82 μH
C_{re}	Secondary compensated capacitor	18.47 nF
C_f	Filter capacitor of rectifier	6*220 μF
f_{wpt}	Switching frequency of the inverter	85 kHz
$U_{in,}$	Input voltage	15, 20 V
U_o	Output voltage	24 V
P	System power level	30-60W
R	Equivalent load resistance	10-20 Ω
k	Coupling coefficient	-0.1~ 0.3

C. MPC with Current Limitation

The current limitation can also be achieved using the polynomial fitting method. The optimal duty cycle can be calculated directly by (25). Thus, the output voltage can track the reference voltage. Similarly, the inductor current at $(n+2)T_s$ can also be expanded as

$$i_{L(n+2)}^{pre} = f_{11} i_{L(n+1)}^{pre} + f_{12} u_{c(n+1)}^{pre} + g_{11}(d_{n+1}) U_{bi} \tag{28}$$

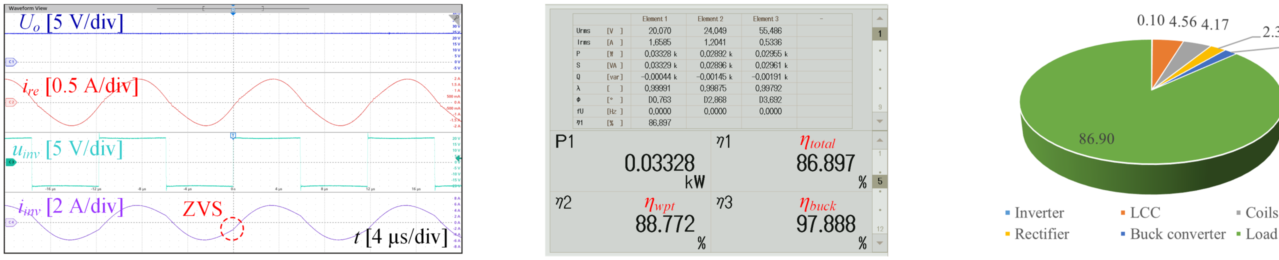

Fig. 10. Steady-state measurement when the receiver is at X=990, U_{in} = 20 V. (a) Steady-state waveform, R_L =10 Ω. (b) System efficiency, U_{in} = 20 V, V_{ref} = 24 V, and R_L =20 Ω. (c) Loss analysis, U_{in} = 20 V, V_{ref} = 24 V, and R_L =20 Ω. (Unit: %).

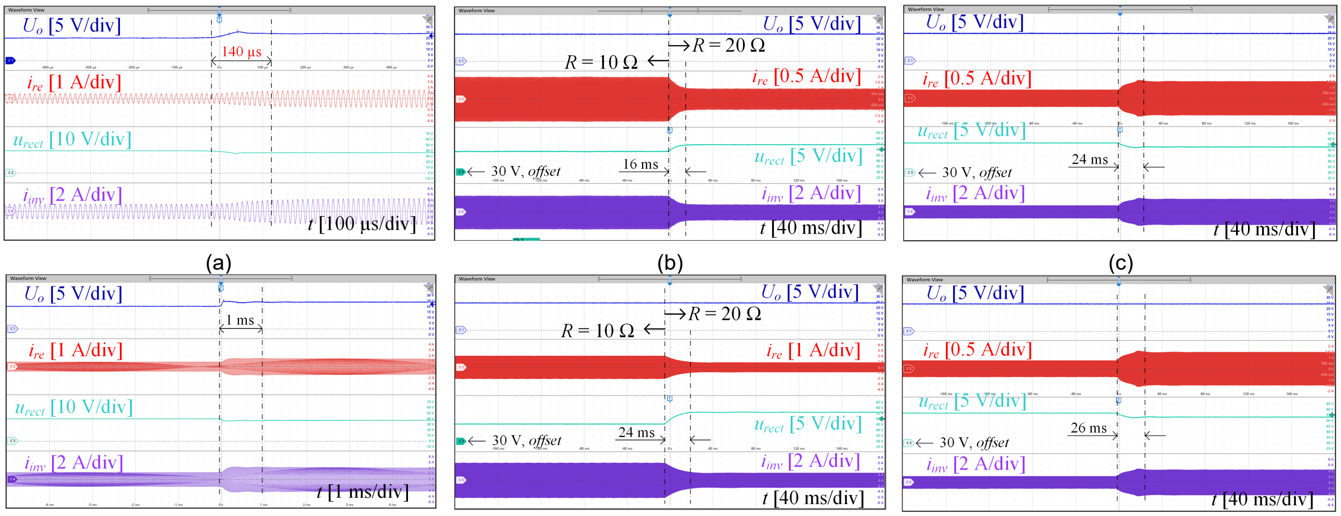

Fig. 11. Experimental waveforms when the receiver is at X=990, U_{in} = 20 V. (a) Reference voltage stepping from 20 to 24 V, R_L =20 Ω (MPC). (b) Load resistor stepping from 10 to 20 Ω, U_{in} = 20 V (MPC). (c) Load current stepping from 1 to 2A, V_{ref} = 24 V (MPC). (d) Reference voltage stepping from 20 to 24 V, R_L =20 Ω (PI controller, Kp = 800, Ki = 100000). (e) Load resistor stepping from 10 to 20 Ω, U_{in} = 20 V, (PI controller, Kp = 800, Ki = 100000). (f) Load current stepping from 1 to 2 A, U_{in} = 20 V (PI controller, Kp = 800, Ki = 100000).

The duty cycle should be limited to constrain the inductor current. The range of duty cycle should follow (29) if the inductor current limitation is I_{lim}, i.e.,

$$f_{11} i_{L(n+1)}^{pre} + f_{12} u_{c(n+1)}^{pre} + g_{11}\left(d_{n+1}\right) U_{bi} \le I_{lim} \tag{29}$$

Consider g_{11} can be fitted by a linear function in (16), the duty cycle can be solved directly, i.e.,

$$d_{n+1} \le \left[\left(I_{lim} - f_{11} i_{L(n+1)}^{pre} - f_{12} u_{c(n+1)}^{pre}\right)\Big/U_{bi} - q_2\right]\Big/q_1 \tag{30}$$

Therefore, the MPC with current limitations can be realized by solving (26) and (30) together.

D. Comparison with Traditional MPC

The flow charts of the proposed MPC and traditional MPC are shown in Fig. 7. The obvious difference is that the optimal duty cycle can be solved by (27) directly for the proposed MPC, and a loop is needed to find the minimum value of the cost function by an optimization algorithm for traditional MPC. Obviously, the computational burden is lower for the method with a direct solution. In addition, although they follow the same steps of predicting voltage and current, the calculation complexity will be reduced further by replacing the matrix exponential with simple polynomial functions.

V. Verification by Experiments

The operating principles have been illustrated in the above section. Experimental setups with five transmitters and one

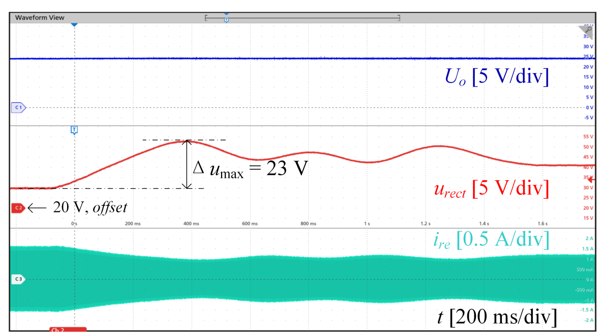

Fig. 12. The experimental waveform when the receiver is moving from X=510 mm to X = 1100 mm, U_{in} = 15 V and R_L =20 Ω.

receiver have been built to verify the proposed MPC in the DWC system, as shown in Fig. 8. The whole setup is 2000 mm long and 400 mm wide, and the vertical distance between the transmitters and receiver coils is 100 mm. Half-bridge module EPC9035 is used to build the full-bridge inverters and the buck converter. The receiver pad can move along the guide rail by the program. The DWC system parameters in experiments are shown in TABLE III, and the parameters of the buck converter are the same as in TABLE II. Five transmitters have similar parameters. When the receiver pad moves along the guide rail, the mutual inductance will change with the position, as shown in Fig. 9. The horizontal coordinate X shows the position of the receiving coil. There is a limit switch at the origin X = 0 mm,

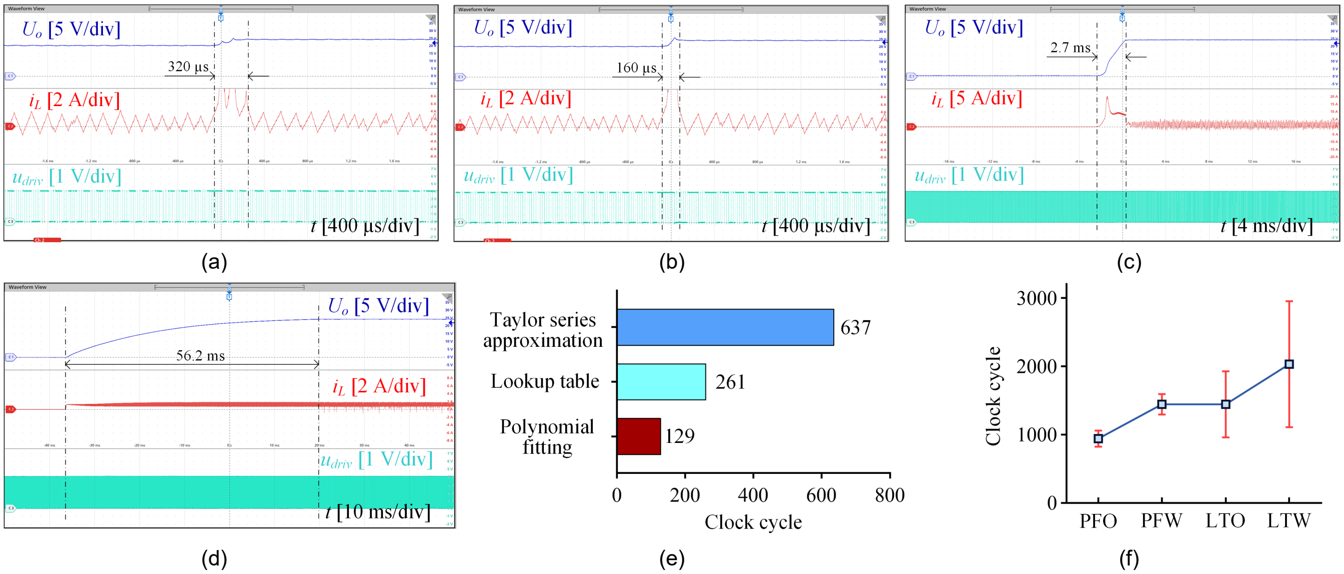

Fig. 13. Comparison between the proposed MPC and other methods. (a) Reference voltage stepping from 20 to 24 V (Lookup table-MPC). (b) Reference voltage stepping from 20 to 24 V (Proposed MPC). (c) Startup using MPC without current limitation. (d) Startup using MPC with current limitation, I_{lim} = 1.05A. (e) Computational overhead comparison for matrix calculation. (f) Computational overhead comparison of code in DSP (PFO: Polynomial fitting MPC without current limitation, PFW: Polynomial fitting MPC with current limitation, LTO: Lookup table MPC without current limitation, and LTW: Lookup table MPC with current limitation)

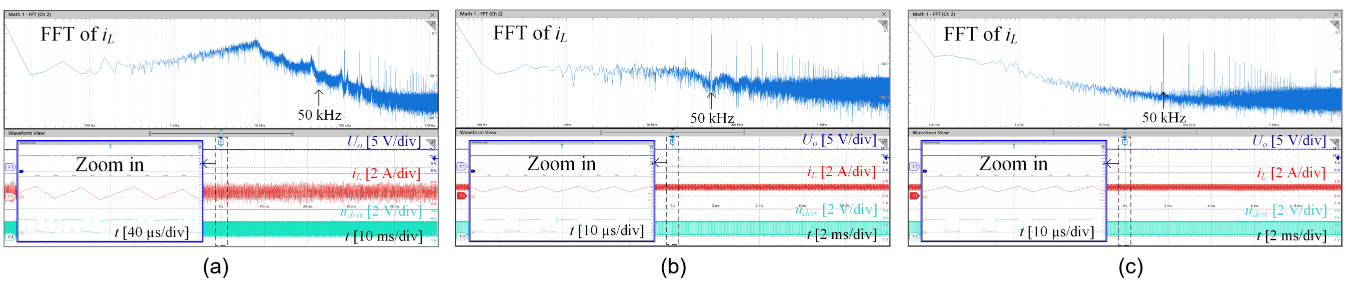

Fig. 14. FFT analysis of the inductor current of the buck converter, U_{bi} = 40 V, V_{ref} = 24 V, and R_L = 20 Ω. (a) Proposed MPC without current limitation. (b) Proposed MPC with current limitation. (c) Conventional PI control.

TABLE IV. COMPARISON OF CONTROL METHODS OF THE WPT SYSTEM

Reference	Method	Parameter sensitivity	Computational burden	Response speed	Implementation complexity
[21]	Passivity-based PI control	Low	Low	Low	Moderate
[29]	H ∞ control	High	High	High	High
[30]	Sliding mode control	High	Moderate	High	Moderate
[31]	Continuous control set-MPC	Moderate	High	High	High
[32]	Finite control Set-MPC	Moderate	High	Moderate	High
[24]	Lookup table-MPC	Moderate	Moderate	Moderate	High
This work	Polynomial fitting-MPC	Moderate	Low	High	Low

and the centers of the five transmitting coils are at X = 520, 680, 840, 1000, and 1160 mm. The range of coupling coefficient between transmitters and receiver is from -0.1 to 0.3. The coupling coefficient is larger than zero when the receiver is close to the transmitter; otherwise, it is smaller than zero. Because the direction of the magnetic flux has changed when the receiver goes away from the transmitter. This phenomenon can also be found in [14].

Experiments for different work conditions have been performed to verify the effectiveness of MPC. The experiment conditions are the same as TABLE II and TABLE III, and the differences are declared before use. The steady-state waveforms are measured when the receiver is stationary on the top of the transmitter 4, X = 990 mm, as shown in Fig. 10(a). The output voltage U_o is 24 V, a commonly used charging voltage for the battery in a light load AGV. The current of the receiving coil i_{re} illustrates that the compensation network can keep the 85 kHz component and filter out other frequencies. In addition, u_{inv} and i_{inv} are the output voltage and current of the inverter connected with transmitter 4, and the voltage phase is ahead of the current phase, which meets the requirement of zero-voltage switching (ZVS). The system efficiency is measured by WT5000, as shown in Fig. 10(b). The whole system's dc-dc efficiency is 86.90%, the dc-dc efficiency of the WPT system is 88.77%, and the efficiency of the buck converter is 97.89%. The loss analysis is shown in Fig. 10(c). The main losses are generated by the LCC network and coupling coils. Therefore, the system efficiency can be improved further by optimizing the LCC network and coils.

A dynamic experiment has also been conducted, as shown in Fig. 12. The receiver moves from transmitter 1 to 5 (X = 510-1100 mm). The output voltage is stable at 24 V, although the output voltage of the rectifier u_{rect} and receiver current i_{re} have significant fluctuations. It can be found that the maximum variation of the output voltage of the rectifier is up to 23 V, and the average of u_{rect} is about 45 V, which means the variation accounts for 51% of u_{rect}. Therefore, the performance of MPC against mutual inductance variation is verified. The voltage fluctuation can be caused by the receiver movement along the X-axis and Y-axis. MPC recognizes voltage fluctuations and suppresses them, but it does not care about the cause of voltage fluctuations. Thus, only dynamic experiments in which the receiver moves along the X-axis are illustrated.

Transient experiments have been conducted to prove the fast response of MPC. First, MPC is compared with PI control by experiments of reference voltage stepping, load resistor stepping, and load current stepping, as shown in Fig. 11. When the reference voltage steps from 20 to 24 V, as shown in Fig. 11(a) and (d). The adjustment time is about 140 µs (around seven switching cycles), which is much shorter than the one of PI control, the experiments of the load resistor step (Fig. 11(b) and (e)) and current step (Fig. 11(c) and (f)) also prove the fast dynamic response of proposed MPC, and a similar conclusion has been offered in [27], [28]. Meanwhile, the proposed MPC with polynomial fitting has a faster dynamic response than the MPC with the lookup table method [24], which can be reflected in comparison experiments of reference voltage stepping, as shown in Fig. 13(a) and (b). The adjustment time of the MPC with the lookup table method is 160 µs, double that of the proposed MPC. The inductor current saturation occurs in these two kinds of MPCs when reference voltage steps due to the quite short adjustment time and the low saturation current of the selected inductor. MPC with current limitations can effectively constrain current and protect the system. However, it can also impact on dynamic response. For instance, the inductor current saturation occurs during the startup of the buck converter (Fig. 13(c)); it can be avoided by limiting the inductor current. Whereas the response time of MPC with current limitation is much larger than that of MPC without current limitation (Fig. 13(d)). Therefore, the VA rating of components should increase if a fast dynamic response is required.

Another important concern of MPC is that matrix exponential calculation in the digital controller will consume significant time and increase the computational burden, which is a critical issue to address for MPC. The clock cycles for matrix calculation in the following two switching periods are tracked in DSP, and the polynomial fitting proposed in this work, lookup table method, and Taylor series approximation are compared in Fig. 13(e). MPC in this work can save at least 50.6% and 79.7% time compared with the lookup table method and Taylor series approximation. The DSP used in experiments is TMS320F28377D, and its clock frequency is 200 MHz. In addition, the clock cycle is also watched when the system is working. Finding the optimal duty cycle and limiting the inductor current will require some loop and judgment statements in the DSP, so the program run time is not fixed. Statistical data results of the polynomial fitting method and lookup table method with and without current limitation are reflected in Fig. 13(f), where the squares represent the mean, and the red line represents the standard deviation. MPC with polynomial fitting has a smaller mean and standard deviation.

In addition, the FFT of the inductor current is shown in Fig. 14. The proposed MPC with and without current limitation and PI control are compared together, and the sampling and control frequency is 50 kHz. The current limitation can help MPC reduce the ripple of the inductor. MPC without current limitation has a bigger ripple than PI control because the solution of the optimal duty cycle in (26) is limited between 0 and 1. Meanwhile, the errors during sampling also cause an inaccurate solution of the optimal duty cycle. Meanwhile, the proposed MPC is compared with other control strategies of the WPT system in multiple aspects, as shown in TABLE IV.

VI. Conclusion

In this paper, a low-computational-burden MPC approach that utilizes a polynomial fitting method based on the parsing solution of the sampled-data model is proposed. The method is applied to the buck converter on the secondary side of DWC systems, where no communication link is needed. The proposed method has been proven to have high accuracy, with an SSE of less than 7.45×10^{-9}. The proposed MPC reduces the calculation complexity by replacing the matrix exponential with polynomial functions. Moreover, the optimal duty cycle can be calculated by solving a quadratic function instead of solving a cost function using an optimization algorithm, which can minimize the computational burden of digital controllers. As a result, the matrix calculation time in two-step prediction is reduced by 50.6% and 79.7% compared to the lookup table method and Taylor series approximation, respectively, and the code running time in DSP of the proposed MPC is shorter than that of MPC with lookup table method. This feature is particularly desirable for high-frequency operations. The proposed approach effectively suppresses output power fluctuations on the secondary side of the DWC system, and it demonstrates a better dynamic performance than PI control through experiments of reference voltage stepping, load resistor stepping, and load current stepping. Furthermore, the system can be protected by adding a current limitation for MPC, and experiments illustrate a neat spectrum and small ripple but large response time.

References

[1] J. Park et al., “A Resonant Reactive Shielding for Planar Wireless Power Transfer System in Smartphone Application,” *IEEE Trans. Electromagn. Compat.*, vol. 59, no. 2, pp. 695–703, Apr. 2017.

[2] M. Xiong, X. Wei, Y. Huang, Z. Luo, and H. Dai, “Research on Novel Flexible High-Saturation Nanocrystalline Cores for Wireless Charging Systems of Electric Vehicles,” *IEEE Trans. Ind. Electron.*, vol. 68, no. 9, pp. 8310–8320, Sept. 2021.

[3] C. Jiang, K. T. Chau, C. Liu, C. H. T. Lee, W. Han, and W. Liu, “Move-and-Charge System for Automatic Guided Vehicles,” *IEEE Trans. Magn.*, vol. 54, no. 11, pp. 1–5, Nov. 2018.

[4] V. Prasanth and P. Bauer, “Distributed IPT Systems for Dynamic Powering: Misalignment Analysis,” *IEEE Trans. Ind. Electron.*, vol. 61, no. 11, pp. 6013–6021, Nov. 2014.

[5] X. Mou and H. Sun, “Analysis of Multiple Segmented Transmitters Design in Dynamic Wireless Power Transfer for Electric Vehicles Charging,” *Electron. Lett.*, vol. 53, no. 14, pp. 941–943, Jul. 2017.

[6] C. Jiang, K. T. Chau, C. Liu, and C. H. T. Lee, “An Overview of Resonant Circuits for Wireless Power Transfer,” *Energies*, vol. 10, no. 7, p. 894, Jun. 2017.

[7] S. Wang, J. Chen, Z. Hu, C. Rong, and M. Liu, “Optimisation Design for Series–Series Dynamic WPT System Maintaining Stable Transfer Power,” *IET Power Electron.*, vol. 10, no. 9, pp. 987–995, Jun. 2017.

[8] K. Chen, J. Pan, Y. Yang, and K. W. E. Cheng, “Stability Improvement and Overshoot Damping of SS-Compensated EV Wireless Charging

Systems with User-End Buck Converters," *IEEE Trans. Veh. Technol.*, vol. 71, no. 8, pp. 8354–8366, Aug. 2022.
[9] W. Zhang, S. Wong, C. K. Tse, and Q. Chen, "Analysis and Comparison of Secondary Series- and Parallel-Compensated Inductive Power Transfer Systems Operating for Optimal Efficiency and Load-Independent Voltage-Transfer Ratio," *IEEE Trans. Power Electron.*, vol. 29, no. 6, pp. 2979-2990, Jun. 2014.
[10] A. Babaki, S. Vaez-Zadeh, A. Zakerian, and G. A. Covic, "Variable-Frequency Retuned WPT System for Power Transfer and Efficiency Improvement in Dynamic EV Charging with Fixed Voltage Characteristic," *IEEE Trans. Energy Convers*., vol. 36, no. 3, pp. 2141-2151, Sept. 2021.
[11] S. Komeda and H. Kifune, "Constant Load Voltage Characteristics in a Parallel-Parallel-Compensated Wireless Power Transfer System," in *Proc. of 2019 10th Int. Conf. on Power Electron. and ECCE Asia (ICPE 2019 - ECCE Asia)*, 2019, pp. 2252–2257.
[12] Y. Yao, Y. Wang, X. Liu, F. Lin, and D. Xu, "A Novel Parameter Tuning Method for a Double-Sided LCL Compensated WPT System with Better Comprehensive Performance," *IEEE Trans. Power Electron.*, vol. 33, no. 10, pp. 8525-8536, Oct. 2018.
[13] H. Feng, T. Cai, S. Duan, J. Zhao, X. Zhang, and C. Chen, "An LCC-Compensated Resonant Converter Optimized for Robust Reaction to Large Coupling Variation in Dynamic Wireless Power Transfer," *IEEE Trans. Ind. Electron.*, vol. 63, no. 10, pp. 6591-6601, Oct. 2016.
[14] F. Lu, H. Zhang, H. Hofmann, and C. C. Mi, "A Dynamic Charging System with Reduced Output Power Pulsation for Electric Vehicles," *IEEE Trans. Ind. Electron*., vol. 63, no. 10, pp. 6580–6590, Oct. 2016.
[15] X. Zhang, Z. Yuan, Q. Yang, Y. Li, J. Zhu and Y. Li, "Coil Design and Efficiency Analysis for Dynamic Wireless Charging System for Electric Vehicles," *IEEE Trans. Magn.*, vol. 52, no. 7, pp. 1-4, Jul. 2016.
[16] Y. Li et al., "A New Coil Structure and Its Optimization Design with Constant Output Voltage and Constant Output Current for Electric Vehicle Dynamic Wireless Charging," *IEEE Trans. Ins. Inform*., vol. 15, no. 9, pp. 5244-5256, Sept. 2019.
[17] H. Li, Y. Liu, K. Zhou, Z. He, W. Li and R. Mai, "Uniform Power IPT System with Three-Phase Transmitter and Bipolar Receiver for Dynamic Charging," *IEEE Trans. Power Electron.*, vol. 34, no. 3, pp. 2013-2017, Mar. 2019.
[18] K. Shi, C. Tang, Z. Wang, X. Li, Y. Zhou, and Y. -J. Fei, "A Magnetic Integrated Method Suppressing Power Fluctuation for EV Dynamic Wireless Charging System," *IEEE Trans. Power Electron.*, vol. 37, no. 6, pp. 7493-7503, Jun. 2022.
[19] P. K. S. Jayathurathnage, A. Alphones, D. M. Vilathgamuwa, and A. Ong, "Optimum Transmitter Current Distribution for Dynamic Wireless Power Transfer with Segmented Array," *IEEE Trans. Microw. Theory Tech.*, vol. 66, no. 1, pp. 346–356, Jan. 2018.
[20] H. Zhu, B. Zhang and L. Wu, "Output Power Stabilization for Wireless Power Transfer System Employing Primary-Side-Only Control," *IEEE Access*, vol. 8, pp. 63735-63747, Mar. 2020.
[21] J. Liu, Z. Liu, and H. Su, "Passivity-Based PI Control for Receiver Side of Dynamic Wireless Charging System in Electric Vehicles," *IEEE Trans. Ind. Electron.*, vol. 69, no. 1, pp. 783–794, Jan. 2022.
[22] Q. Xu, Y. Yan, C. Zhang, T. Dragicevic, and F. Blaabjerg, "An offset-free composite model predictive control strategy for DC/DC buck converter feeding constant power loads," *IEEE Trans. Power Electron*., vol. 35, no. 5, pp. 5331–5342, May 2020.
[23] L. Chen et al., "Moving discretized control set model-predictive control for dual-active bridge with the triple-phase shift," *IEEE Trans. Power Electron.,* vol. 35, no. 8, pp. 8624–8637, Aug. 2020.
[24] G. Gao et al., "Model predictive control of dual active bridge converter based on the lookup table method," in *Proc. IEEE 10th Int. Symp. Power Electron. for Distrib. Gener. Syst. (PEDG)*, Jun. 2019, pp. 183–186.
[25] P. Falkowski and A. Sikorski, "Finite control set model predictive control for grid-connected AC–DC converters with LCL filter," *IEEE Trans. Ind. Electron.,* vol. 65, no. 4, pp. 2844–2852, Apr. 2018.
[26] A. Alkasir, S. E. Abdollahi, S. R. Abdollahi, and P. Wheeler, "Enhancement of dynamic wireless power transfer system by model predictive control," *IET Power Electron.*, vol. 15, no. 1, pp. 67-79, Jan. 2022.
[27] S. Liu et al., "Dynamic Improvement of Inductive Power Transfer Systems with Maximum Energy Efficiency Tracking Using Model Predictive Control: Analysis and Experimental Verification," *IEEE Trans. Power Electron.*, vol. 35, no. 12, pp. 12752–12764, Dec. 2020.
[28] Z. Zhou, L. Zhang, Z. Liu, Q. Chen, R. Long, and H. Su, "Model Predictive Control for the Receiving-Side DC–DC Converter of Dynamic Wireless Power Transfer," *IEEE Trans. Power Electron.*, vol. 35, no. 9, pp. 8985–8997, Sept. 2020.
[29] Z. Tang, W. Xiao, B. Zhang, D. Qiu, F. Xie, and Y. Chen, "H-infinity loop shaping control of wireless power transfer system based on generalized state space averaging model," *Int. J. Circ. Theor. Appl*., early access. doi: 10.1002/cta.3772.
[30] Y. Yang, W. Zhong, S. Kiratipongvoot, S. -C. Tan, and S. Y. R. Hui, "Dynamic Improvement of Series–Series Compensated Wireless Power Transfer Systems Using Discrete Sliding Mode Control," *IEEE Trans. Power Electron*., vol. 33, no. 7, pp. 6351–6360, Jul. 2018.
[31] A. Alkasir, S. Ehsan Abdollahi, S. Reza Abdollahi, and P. Wheeler, "A Primary Side CCS-MPC Controller for Constant Current/Voltage Charging Operation of Series-Series Compensated Wireless Power Transfer Systems," in *Proc. of 2021 12th Power Electron, Drive Systems, and Technologies Conference (PEDSTC)*, 2021, pp. 1–5.
[32] S. Chen, W. Ding, L. Huo, X. Wu, S. Shi, and R. Hu, "Dynamic Improvement and Efficiency Optimization of Wireless Power Transfer Systems Using Improved FCS-MPC and P&O Methods," *IEEE Trans. Power Electron.,* vol. 38, no. 11, pp. 14702-14718, Nov. 2023.

Tianlu Ma (Student Member, IEEE) received the B.Eng. degree in electrical engineering and automation from Jilin University, Changchun, China, in 2018, and the M.Sc. degree in electrical engineering from Xi'an Jiaotong University, Xi'an, China, in 2021. He is currently working toward the Ph.D. degree in electrical engineering at City University of Hong Kong, Hong Kong.

His research interests include wireless power transfer modeling and control, and power electronics.

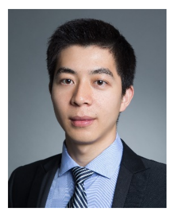

C. Q. Jiang (Senior Member, IEEE) received the B.Eng. and M.Eng. degrees (First Class Honours) in Electrical Engineering and Automation from Wuhan University, Wuhan, China, in 2012 and 2015, respectively, and the Ph.D. degree in Electrical and Electronic Engineering from The University of Hong Kong, Hong Kong SAR, China, in 2019.

He is currently an Assistant Professor with the Department of Electrical Engineering, Faculty Member with the State Key Laboratory of Terahertz and Millimeter Waves, City University of Hong Kong, Hong Kong, SAR, China. Since 2021, he has also been with Clare Hall, University of Cambridge. From 2019 to 2021, he was a Postdoctoral Research Associate with the University of Cambridge, Cambridge, U.K. In 2019, he was a Visiting Researcher with the Nanyang Technological University, Singapore. His research interests include power electronics, wireless power transfer techniques, electric machines and drives, and electric vehicle technologies.

Dr. Jiang was the recipient of the Winner, CAPE Acorn Blue Sky Research Award at the University of Cambridge and First Prize in the Interdisciplinary Research Competition at the University of Hong Kong. He is currently an Associate Editor for IET Renewable Power Generation, and the Guest Editor of Energies and IEEE Open Journal of Vehicular Technology.

Chen Chen received the B.Eng. and M.Eng. degrees in Mechanical Manufacture and Automation from Wuhan University of Technology, Wuhan, China, in 2019 and 2022, respectively. He is currently working toward the Ph.D. degree in the Department of Electrical and Electronic Engineering, The City University of Hong Kong, Hong Kong.

His research interests include wireless power transfer techniques, electric machines, and devices.

Yibo Wang received the B.Eng degree in automation from Nankai University, Tianjin, China, in 2016 and the M.Sc. degree in electrical power engineering from RWTH Aachen University, Aachen, Germany, in 2019. He is currently pursuing his Ph.D. degree in the Department of Electrical and Electronics Engineering, The City University of Hong Kong, Hong Kong.

He was a hardware development engineer with Delta Energy Systems (Germany) GmbH from 2019 to 2022. His research interests include wireless power transfer, electric vehicles, and power electronics.

Jiayi Geng received the B.Eng. degree and M.Sc. degree in electrical engineering and automation from Hebei University of Technology, Tianjin, China, in 2019 and 2022, respectively. She is currently a research assistant with the Department of Electrical Engineering, City University of Hong Kong, Hong Kong SAR, China.

Her research interests include DC-DC converters, condition monitoring of WBG power devices, and power electronics.

Chi K. Tse (Fellow, IEEE) received the B.Eng. (Hons.), with first-class honors, and the Ph.D. degrees in electrical engineering from the University of Melbourne, Parkville, VIC, Australia, in 1987 and 1991, respectively.

He is currently an Associate Vice President (Innovation) and Chair Professor of Electrical Engineering with the City University of Hong Kong, Hong Kong. His research interests include power electronics, nonlinear systems, and complex network applications.

Dr. Tse was the recipient of a number of research and invention prizes, including the IEEE CASS Charles A. Desoer Technical Achievement Award in 2022, and a few Best Paper Prizes from IEEE and other journals, as well as a Grand Prize and Gold Medal in Silicon Valley International Invention Festival 2019. He has been appointed to honorary professorship and distinguished fellowship by a few Australian, Canadian, and Chinese universities, including the Chang Jiang Scholar Chair Professor with the Huazhong University of Science and Technology, Honorary Professor of Melbourne University, and Distinguished Professor-at-Large with the University of Western Australia. He was a Panel Member of Hong Kong Research Grants Council, and Member of several professional and government committees. In 2005, 2010, and 2018, he was selected as an IEEE Distinguished Lecturer. In 2006, he chaired the IEEE CAS Technical Committee on Nonlinear Circuits and Systems. He is and was the Editor-in-Chief of IEEE Transactions on Circuits and Systems II (2016–2019), IEEE Circuits and Systems Magazine (2013–2016), and IEICE Nonlinear Theory and Applications (since 2013), an Associate Editor for a few other IEEE journals, and on the Editorial Board of IEEE Proceedings (2021–2022). He was on a number of IEEE committees, including the IEEE Fellows Committee and the IEEE Awards Committee, and chaired the Steering Committee for IEEE Transactions on Network Science and Engineering.